Optics & Laser Technology 44 (2012) 528–533

Contents lists available at SciVerse ScienceDirect

Optics & Laser Technology

journal homepage: www.elsevier.com/locate/optlastec

Analysis of non-linear refractive index influences on four-wave mixing conversion efficiency in semiconductor optical amplifiers

S.R. Hosseini [a], M. Razaghi [a,*], N.K. Das [b]

[a] Department of Electrical and Computer Engineering, University of Kurdistan, Parsadian Avenue, Sanandaj, Iran
[b] Department of Electrical and Computer Engineering, Curtin University, Perth, WA 6845, Australia

ARTICLE INFO

Article history:
Received 15 March 2011
Received in revised form
20 August 2011
Accepted 23 August 2011
Available online 28 September 2011

Keywords:
Semiconductor optical amplifier
Non-linear refractive index
Four-wave mixing

ABSTRACT

In this paper, we have analyzed the influences of non-linear refractive index on the four-wave mixing (FWM) characteristics in semiconductor optical amplifiers (SOAs). It has been shown that the generated FWM signal characteristics can be modified due to the variation of non-linear refractive index of the SOA's medium. The wave propagation in the SOA has been modeled using the nonlinear propagation equation taking into account gain spectrum dynamics, gain saturation, which depends on carrier depletion, carrier heating, spectral hole-burning, group velocity dispersion, self-phase modulation and two photon absorption. Simulation of optical wave evolution in the SOA has been carried out using the finite-difference beam propagation method (FD-BPM) both in time and spectral domains. Our simulation results confirm that higher FWM conversion efficiency and lower time bandwidth product are achieved for higher absolute values of non-linear refractive index. Moreover, non-linear refractive index is more efficacious for high power propagated waves in SOAs. Finally, we have studied the modification of waveguide refractive index due to the propagation of optical pulses. We have also shown that when $|n_2|=1$ cm^2/TW, refractive index variation is in the order of 10^{-4} to 10^{-7} for high and low power input pulses, respectively.

1. Introduction

Four-wave mixing (FWM) in semiconductor optical amplifiers (SOAs) is an attractive phenomena for wavelength conversion [1,2]. All-optical devices using FWM in SOAs have certain important features, such as optical gain, operation with relatively low optical input power, small size and capability of large-scale integration [3,4]. The operation of these devices is expected to be all-optical (e.g., wavelength conversion, optical demultiplexing and optical sampling) [5].

The fast non-linear phenomena occurring in the SOA medium affect the FWM process in the SOA. One of these non-linear phenomena is optical Kerr effect, which is an instantaneous non-linear response that can be described as modifying the refractive index of the SOA medium [6]. The strength of the Kerr non-linearity and the magnitude of non-linear refractive index (n_2) in the waveguide of the SOA is usually measured using interferometric techniques [7].

Recently, several theoretical models have reported the optical wave propagation in SOAs [8–15]. In these reports, most of the existing models have considered non-linear refractive index as an influential parameter, which affects the optical wave propagation in SOAs. However, the impact of non-linear refractive index on the FWM characteristics in SOAs has not been analyzed in detail in previous reported works. Therefore, analysis of nonlinear refractive index's (Kerr effect) influences on FWM characteristics and FWM conversion efficiency in SOAs is an important issue for designing an accurate communication system.

The main objective of this paper is to investigate the influences of non-linear refractive index (Kerr effect) parameter on the non-degenerate FWM characteristics among short optical pulses in SOAs. To obtain our goal, we have numerically simulated the optical wave evolution in an SOA. Our analysis is based on the modified nonlinear Schrödinger equation considering self-phase modulation (SPM), two-photon absorption (TPA), group velocity dispersion (GVD), carrier depletion (CD), carrier heating (CH), spectral-hole burning (SHB), gain spectrum dynamics and gain saturation in an SOA [8–10]. We used the finite-difference beam propagation method (FD-BPM) for simulation, because of short convergence time and excellent accuracy of the results [8,9].

This paper is organized as follows: Section 1 is Introduction; Section 2 is Analytical Model, the equations, which govern the dynamics of the amplification process; Section 3 is Simulation results and discussion and finally Conclusions are in Section 4.

2. Analytical model

The model we have used is based on the modified nonlinear Schrödinger equation, which explains the propagation of optical

* Corresponding author.
E-mail addresses: m.razaghi@uok.ac.ir, mrazaghi@gmail.com (M. Razaghi).

0030-3992/$ - see front matter © 2011 Elsevier Ltd. All rights reserved.
doi:10.1016/j.optlastec.2011.08.016

pulses in the SOA's medium [9].

$$\left[\frac{\partial}{\partial z}-\frac{i}{2}\beta_2\frac{\partial^2}{\partial\tau^2}+\frac{\gamma}{2}+\left(\frac{\gamma_{2p}}{2}+ib_2\right)|V(z,\tau)|^2\right]V(z,\tau)=\left\{\frac{1}{2}g_N(\tau)\left[\frac{1}{f(\tau)}+i\alpha_N\right]+\frac{1}{2}\Delta g_T(\tau)(1+i\alpha_T)-i\frac{1}{2}\frac{\partial g(\tau,\omega)}{\partial\omega}\Big|_{\omega_0}\frac{\partial}{\partial\tau}-\frac{1}{4}\frac{\partial^2 g(\tau,\omega)}{\partial\omega^2}\Big|_{\omega_0}\frac{\partial^2}{\partial\tau^2}\right\}V(z,\tau) \tag{1}$$

where $V(z,\tau)$ is the complex envelope function of an optical pulse. The definitions of some parameters in the above equation are as follows:

$$g_N(\tau)=g_0\exp\left[-\frac{1}{E_{sat}}\int_{-\infty}^{+\infty}u(s)|V(\tau-s)|^2ds\right] \tag{2}$$

$$f(\tau)=1+\frac{1}{\tau_{shb}P_{shb}}\int_{-\infty}^{\infty}u(s)e^{-s/\tau_{shb}}|V(\tau-s)|^2ds \tag{3}$$

$$\Delta g_T(\tau)=-h_1\int_{-\infty}^{+\infty}u(s)e^{-s/\tau_{ch}}\times(1-e^{-s/\tau_{shb}})|V(\tau-s)|^2ds-h_2\int_{-\infty}^{+\infty}u(s)e^{-s/\tau_{ch}}\times(1-e^{-s/\tau_{shb}})|V(\tau-s)|^4ds \tag{4}$$

$$\frac{\partial g(\tau,\omega)}{\partial\omega}\Big|_{\omega_0}=A_1+B_1[g_0-g(\tau,\omega_0)] \tag{5}$$

$$\frac{\partial^2 g(\tau,\omega)}{\partial\omega^2}\Big|_{\omega_0}=A_2+B_2[g_0-g(\tau,\omega_0)] \tag{6}$$

$$g(\tau,\omega_0)=g_N(\tau,\omega_0)/f(\tau)+\Delta g_T(\tau,\omega_0) \tag{7}$$

where $\tau=t-z/v_g$ is the local time frame, which propagates with the group velocity v_g of the optical pulse at central frequency. The slowly varying envelope function approximation is used in Eq. (1), where the temporal variation change of the complex envelope function is very slow in comparison to the cycle of an optical field. $|V(z,\tau)|^2$ represents the optical pulse power, β_2 is the group velocity dispersion (GVD), γ is the linear loss, γ_{2p} is the two-photon absorption coefficient, $b_2(=\omega_0 n_2/cA)$ is the instantaneous self-phase modulation term due to the Kerr effect, n_2 is the instantaneous non-linear refractive index, $\omega_0(=2\pi f_0)$ is the center angular frequency of the pulse, c is the velocity of light in vacuum and $A(=wd/\Gamma)$ is the effective area (d and w are the thickness and the width of the active region, respectively, and Γ is the confinement factor). $g_N(\tau)$ is the saturated gain due to carrier depletion, g_0 is the linear gain, E_{sat} is the saturation energy, τ_s is the carrier lifetime, $f(\tau)$ is the spectral hole-burning function, P_{shb} is the spectral hole-burning saturation power, τ_{shb} is the spectral hole-burning relaxation time and α_N and α_T are the linewidth enhancement factors associated with the gain changes due to the carrier depletion and carrier heating. $\Delta g_T(\tau)$ is the resulting gain change due to the carrier heating and two-photon absorption, $u(s)$ is the unit step function, τ_{ch} is the carrier heating relaxation time, h_1 is the contribution of stimulated emission and free-carrier absorption to the carrier heating gain reduction and h_2 is the contribution of two-photon absorption. Finally, A_1 and A_2 are the slope and the curvature of the linear gain at ω_0, respectively, while B_1 and B_2 are constants describing changes in these quantities with saturation [8–10].

In our model, we have included the dynamic gain change terms, i.e. the first-and second-order gain spectrum terms, which are the last two terms of the right side in Eq. (1). We cannot separate the linear propagation term (GVD term) and phase compensation terms (other than GVD, first- and second-order gain spectrum terms) in Eq. (1) for the individual consideration of the time and frequency domain for the optical pulse propagation. Therefore, it is not possible to use the common methods like fast Fourier transformation BPM (FFT-BPM) [9]. Hence, we have applied the FD-BPM [16]. If we replace the time derivative terms of Eq. (1) by the central-difference approximation (8) and integrate Eq. (1) with the small propagation step Δz, we obtain the tridiagonal simultaneous matrix (9):

$$\frac{\partial}{\partial\tau}V_k=\frac{V_{k+1}-V_{k-1}}{2\Delta\tau},\frac{\partial^2}{\partial\tau^2}V_k=\frac{V_{k+1}-2V_k+V_{k-1}}{\Delta\tau^2} \tag{8}$$

$$-a_k(z+\Delta z)V_{k-1}(z+\Delta z)+\{1-b_k(z+\Delta z)\}\times V_k(z+\Delta z)-c_k(z+\Delta z)V_{k+1}(z+\Delta z)=a_k(z)V_{k-1}(z)+\{1+b_k(z)\}V_k(z)+c_k(z)V_{k+1}(z) \tag{9}$$

where $V_k=V(\tau_k)$, $V_{k+1}=V(\tau_k+\Delta\tau)$ and $V_{k-1}=V(\tau_k-\Delta\tau)$ when $k=1,2,3,\ldots,n$ and

$$a_k(z)=\frac{\Delta z}{2}\left[\frac{i\beta_2}{2\Delta\tau^2}+i\frac{1}{4\Delta\tau}\frac{\partial g(\tau,\omega,z)}{\partial\omega}\Big|_{\omega_0,\tau_k}-\frac{1}{4\Delta\tau^2}\frac{\partial^2 g(\tau,\omega,z)}{\partial\omega^2}\Big|_{\omega_0,\tau_k}\right] \tag{10}$$

$$b_k(z)=-\frac{\Delta z}{2}\left[\frac{i\beta_2}{\Delta\tau^2}+\frac{\gamma}{2}+\left(\frac{\gamma_{2p}}{2}+ib_2\right)|V_k(z)|^2-\frac{1}{2}g_N(\tau_k,\omega_0,z)(1+i\alpha_N)-\frac{1}{2}g_N(\tau_k,\omega_0,z)(1+i\alpha_T)-\frac{1}{2\Delta\tau^2}\frac{\partial^2 g(\tau,\omega,z)}{\partial\omega^2}\Big|_{\omega_0,\tau_k}\right] \tag{11}$$

$$c_k(z)=\frac{\Delta z}{2}\left[\frac{i\beta_2}{2\Delta\tau^2}-i\frac{1}{4\Delta\tau}\frac{\partial g(\tau,\omega,z)}{\partial\omega}\Big|_{\omega_0,\tau_k}-\frac{1}{4\Delta\tau^2}\frac{\partial^2 g(\tau,\omega,z)}{\partial\omega^2}\Big|_{\omega_0,\tau_k}\right] \tag{12}$$

where $\Delta\tau$ is the sampling time and n is the number of sampling. If we know $V_k(z)$, $(k=1,2,3,\ldots,n)$ at position z, we can calculate $V_k(z+\Delta z)$ at position of $z+\Delta z$, which is propagation of a step Δz from position z, using (9).

It is not possible to directly calculate (9) because it is necessary to calculate the left-side terms $a_k(z+\Delta z)$, $b_k(z+\Delta z)$ and $c_k(z+\Delta z)$ of (9) from the unknown $V_k(z+\Delta z)$. Therefore, we initially defined $a_k(z+\Delta z)\equiv a_k(z)$, $b_k(z+\Delta z)\equiv b_k(z)$ and $c_k(z+\Delta z)\equiv c_k(z)$. Then, we obtained $V_k^{(0)}(z+\Delta z)$, as the zeroth order approximation of $V_k(z+\Delta z)$ using (9). After that, we substituted $V_k^{(0)}(z+\Delta z)$ in (10) and obtained $V_k^{(1)}(z+\Delta z)$ as the first-order approximation of $V_k(z+\Delta z)$. Finally, we obtained accurate simulation results by iteration [9].

When two optical pulses with different central frequencies of f_p (pump) and f_q (probe) are injected into the SOA simultaneously, the FWM signal is generated in the SOA at a frequency of $2f_p-f_q$ [9]. For the analysis of the nondegenerate FWM characteristics, we have used the following equation to describe two input pulses (pump and probe pulses), which are simultaneously injected into the SOA [9]:

$$V(\tau)=V_p(\tau)+V_q(\tau)\exp(-i\Delta\omega\tau) \tag{13}$$

where $V_p(\tau)$ and $V_q(\tau)$ are the complex envelope functions of the input pump and probe pulses, and $\Delta\omega$ is a detuning angular frequency expressed as $\Delta\omega=2\pi f=2\pi(f_p-f_q)$. Using the complex envelope function of (13), we get the solution of (1) and obtain the propagation characteristics of generated FWM signal in an SOA.

3. Simulation results and discussion

The parameters of a bulk SOA (AlGaAs/GaAs, double heterostructure) with a wavelength of 0.86 μm were used in our simulation as listed in Table 1 [9]. The following results were achieved when the input pulses had sech^2 shape and were Fourier

Table 1
List of parameters of a bulk SOA (AlGaAs/GaAs, double hetero-structure) with a wavelength of 0.86 μm used in simulation [9,20].

L	SOA length	500 μm
A	Effective area	5 μm^2
f_0	Center frequency of the pulse	349 THz
β_2	Group velocity dispersion	0.05 $ps^2\ cm^{-1}$
E_{sat}	Saturation energy	80 pJ
n_0	Linear refractive index	3.6
α_N	Linewidth enhancement factor due to the carrier depletion	3.1
α_T	Linewidth enhancement factor due to the carrier heating	2.0
h_1	Contribution of stimulated emission and free carrier absorption to the carrier heating gain reduction	0.13 $cm^{-1}\ pJ^{-1}$
h_2	Contribution of stimulated emission and free carrier absorption to the carrier heating gain reduction	126 fs $cm^{-1}\ pJ^{-1}$
τ_s	Carrier lifetime	200 ps
τ_{ch}	Carrier heating relaxation time	700 ps
τ_{shb}	Spectral hole burning relaxation time	60 ps
τ_{shb}	Spectral hole burning relaxation power	28.3 W
γ	Linear loss	11.5 cm^{-1}
γ_{2p}	Two photon absorption coefficient	1.1 $cm^{-1}\ W^{-1}$
A_1		0.15 fs μm^{-1}
A_2	Parameters describing the second order	−80 fs
B_1	Taylor expansion of the dynamical gain	−60 $fs^2\ \mu m^{-1}$
B_2	Spectrum	0 fs^2

transform limited. The simulation results were verified through comparison with the previously published works [4,5,8,9].

Based on experimental results, the nonlinear index of refraction will change for several reasons [17–18]. In this simulation, the values of nonlinear refractive index (n_2) ranges from $-0.1\ cm^2/TW$ to $-1\ cm^2/TW$. The simulation was carried out for two types of input optical pulses. First condition is low power (unsaturated gain) regime, where the pump pulse energy is $E_{pump}=10$ fJ and the input probe pulse energy is $E_{probe}=1$ fJ. Second condition is high power (saturated gain) regime, where the input pump pulse energy is $E_{pump}=5$ pJ and the input probe pulse energy is $E_{probe}=500$ fJ.

3.1. FWM characteristics

Fig. 1 shows the waveform of the generated FWM signals for various values of nonlinear refractive index for (a) a low power (unsaturated gain) regime and (b) a high power (saturated gain) regime. In Fig. 1(a), the power of the generated FWM signal is 4.8 nW when the nonlinear refractive index is $-0.1\ cm^2/TW$ and its power increases to 7.2 nW when the value of nonlinear refractive index is $-1\ cm^2/TW$. Fig. 1(b) shows that the peak power of generated FWM signal varies from 12 mW to 22 mW when the nonlinear refractive index varies from $-0.1\ cm^2/TW$ to $-1\ cm^2/TW$. It has been shown clearly that the power of the generated FWM signal increases as the absolute value of the nonlinear refractive index increases. The origin of this power increment comes from the direct relationship between the nonlinear refractive index and the input optical pulse power in (1).

Fig. 1(b) also indicates that the peaks of the generated FWM signals experience two shifts during the propagation in the SOA. The first shift is through the leading edge (negative side) of the pulse and it is mainly due to the faster gain saturation in the SOA and SPM that occur for higher energy input signals [11]. The second shift is due to the trailing edge (positive side) of the pulse and it comes from the variation of nonlinear refractive index. More detail of this peak shift is shown in Fig. 3.

Fig. 2 shows the spectrum of the generated FWM signals for several values of nonlinear refractive index, (a) for low energy input pulses and (b) for high energy input pulses. In the case of high energy input pulses, the peak of the generated FWM

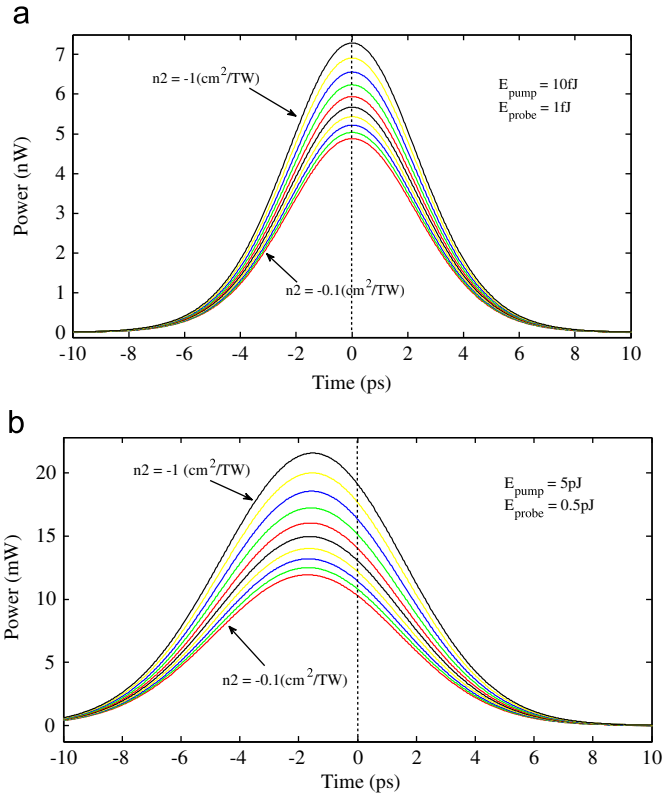

Fig. 1. Waveforms of the generated FWM signals for several values of nonlinear refractive index: (a) for a low power regime and (b) for a high power regime.

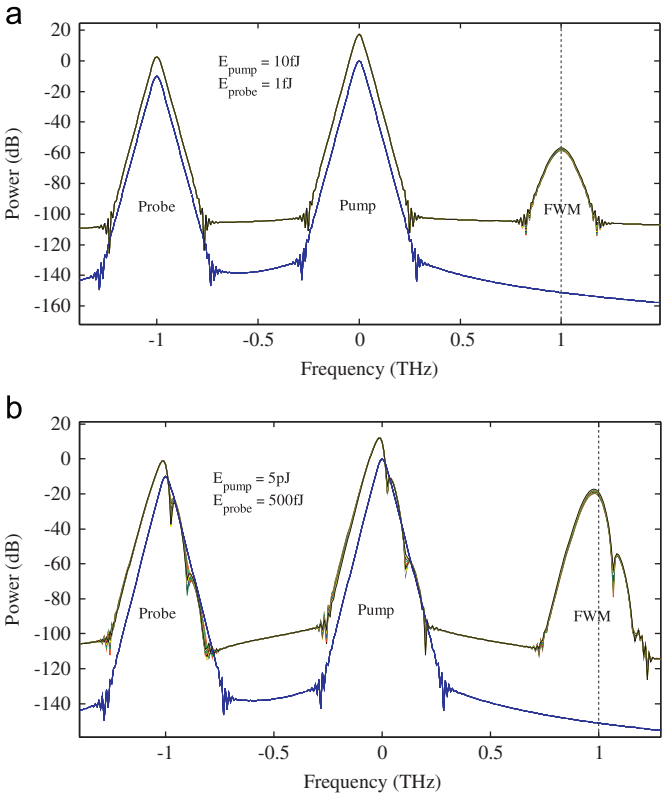

Fig. 2. Spectrum of the generated FWM signals for several values of nonlinear refractive index: (a) for a low power regime and (b) for a high power regime. Peak of the generated FWM spectrum has experienced ~8.3 GHz shift due to the variation of nonlinear refractive index from $-0.1\ cm^2/TW$ to $-1\ cm^2/TW$.

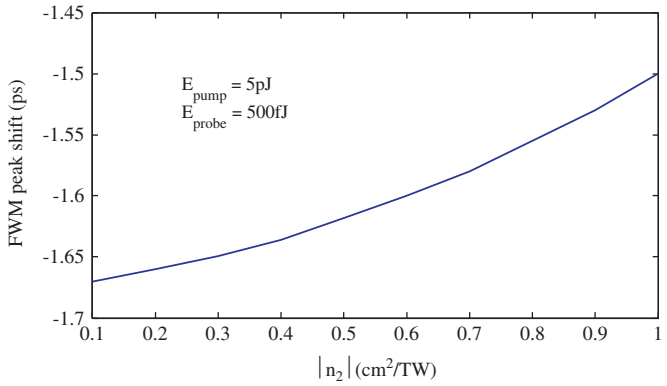

Fig. 3. Peak shift of the generated FWM pulses for various values of nonlinear refractive index in the high power regime.

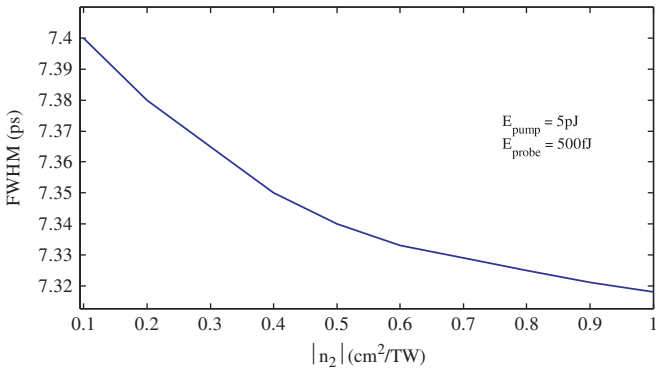

Fig. 4. Full width at half maximum (FWHM) of the generated FWM pulses for various values of nonlinear refractive index in the high power regime.

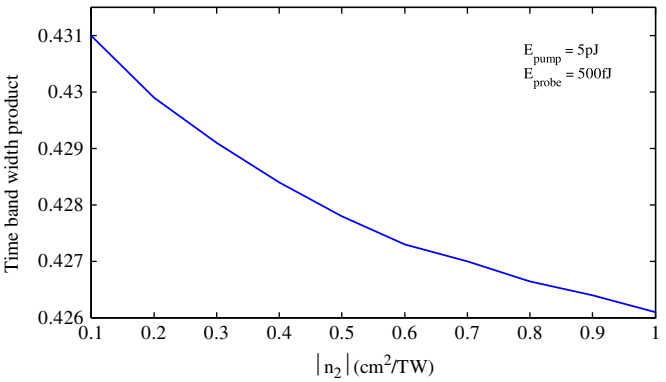

Fig. 5. The time bandwidth product (TBP) of the generated FWM pulses for various values of nonlinear refractive index in the high power regime.

spectrum experienced ~20 GHz shifts to the lower frequency side (red shift) due to the SPM phenomenon [11]. In addition, the peak of the generated FWM signal experienced ~8.3 GHz shifts to the lower frequency side (red shift) by variation of nonlinear refractive index from $n_2 = -0.1$ cm^2/TW to $n_2 = -1$ cm^2/TW. In high power regime, the oscillatory structures are decreased when the absolute value of nonlinear refractive index is increased. It comes from the negative sign of the nonlinear refractive index.

Fig. 3 shows the peak shift of the generated FWM signal for several values of nonlinear refractive index in high power regime. The high energy input pulses impose a shift to generated FWM signal, because the high power input pulses make the SOA saturated and the SPM induces the nonlinear refractive index in the SOA medium [11]. However, with the increase of the absolute value of nonlinear refractive index, the actual value of nonlinear refractive index decreases because of its negative sign. As a result, the peak shift decreases. In other words, external increase of the absolute value of nonlinear refractive index could partly compensate the index of refraction, which is induced by the SPM in the high power regime. The peak position of the generated FWM signal experiences a shift of -1.67 ps when the value of nonlinear refractive index was -0.1 cm^2/TW. The negative sign of peak shift means that the peak position has shifted to the lower values. Besides, the generated FWM signal's peak position experiences -1.5 ps shift when the value of nonlinear refractive index was -1 cm^2/TW.

In the case of low power regime, the peak position of the generated FWM signal has not experienced any shift for different values of nonlinear refractive index. It confirms that the influences of nonlinear phenomena are more noticeable in the high power regime when the SOA is saturated.

Fig. 4 shows the full width at half maximum (FWHM) of the generated FWM signal for different values of nonlinear refractive index in the high power regime. Here, the generated FWM signal has the FWHM of 7.4 ps when the value of nonlinear refractive index is -0.1 cm^2/TW and the FWHM decreases to 7.32 ps when the value of nonlinear refractive index is -1 cm^2/TW. This relationship (Fig. 4) illustrates that the higher absolute value of nonlinear refractive index leads to the lower FWHM of the generated FWM signal. The physics behind this phenomenon is that the amplification of high power pulse with high intensity decreases the density of carriers in conduction band of semiconductor in the SOA cavity. The lower carrier density leads to the lower SOA gain. With the increase in the nonlinear refractive index, the power of the propagated pulse increases (Fig. 1) and the carrier densities decrease further. So, the leading edge of the propagated pulse experiences a lower gain and its FWHM decreases. Decreasing the width of optical pulses is useful in high speed optical communication systems because data can be carried in a shorter width and this leads to faster data processing.

Fig. 5 shows the time-bandwidth product (TBP) of the generated FWM signal for various values of nonlinear refractive index in the high power regime. The TBP of a pulse is defined as the product of its temporal FWHM and the spectral width of the pulse. The TBP of a pulse is often used for representing how close a pulse is to the transform-limited pulse, which is an ideal case (parameter) for optical communication systems [8]. In the high power regime, the TBP of the generated FWM signal is 0.431 when the nonlinear refractive index is -0.1 cm^2/TW and the value of TBP reduces to 0.426 when the value of nonlinear refractive index is -1 cm^2/TW. From Fig. 5, it is clear that the TBP of the generated FWM signal is decreased when the absolute value of nonlinear refractive index is increased. Decreasing the TBP is an appropriate function in amplification process because the pulses with lower TBP are more suitable for optical communication systems.

In the case of low power (energy) input pulses, the TBP of the generated FWM signal remained constant at 0.371 for various values of nonlinear refractive index.

Fig. 6 shows the generated FWM signal energy for several values of nonlinear refractive index, (a) for a low power regime and (b) for a high power regime. In the low power regime, the generated FWM signal energy increased from 0.03 (aJ) to 0.044 aJ when nonlinear refractive index is varied from -0.1 cm^2/TW to -1 cm^2/TW. From Fig. 6(a), it is clear that the FWM signal energy is increased ~47%. But in the high power regime, the generated FWM signal energy increased from 94 fJ to 170 fJ when the nonlinear refractive index varied from -0.1 cm^2/TW to -1 cm^2/TW. From Fig. 6(b), it is clear that the FWM signal energy is

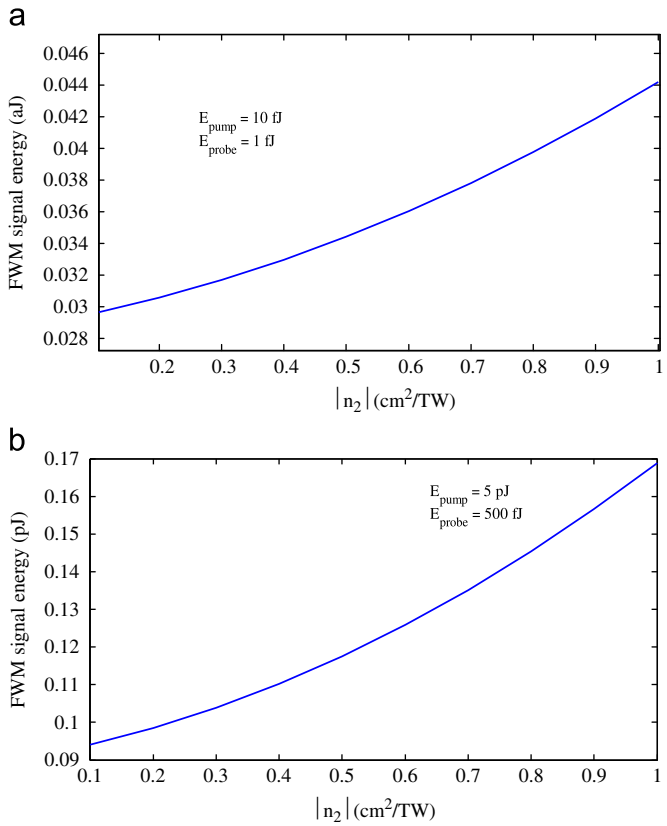

Fig. 6. FWM signal energy for various values of nonlinear refractive index, (a) for low power regime and (b) for a high power regime.

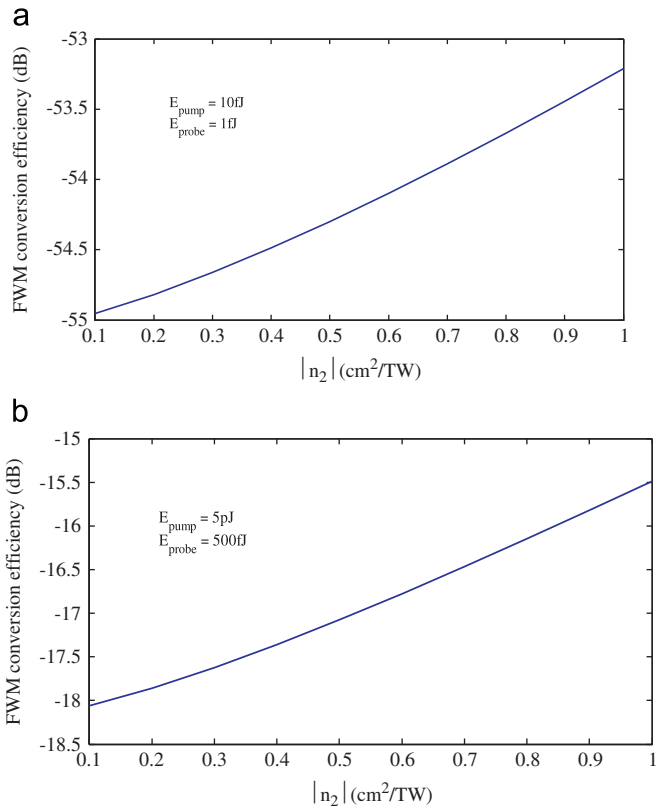

Fig. 7. FWM conversion efficiency for several values of nonlinear refractive index, (a) for a low power regime and (b) for a high power regime.

increased ~81%. Increasing the energy of the generated FWM signal is useful in optical communication applications.

For both conditions the generated FWM signal energy is increased by increasing the absolute value of the nonlinear refractive index. However, the increasing rate is faster for high power regime when the SOA is saturated. It comes from the nonlinear relationship between the intensity of the generated FWM signal and the intensity of input pump and probe pulses. The generated FWM signal intensity is proportional to $I_P^2 I_q$ [9]. Here, I_P is the pump intensity and I_q is the probe intensity. Hence, the generated FWM signal energy will increase further by increasing of the input pump pulse energy.

Fig. 7 shows the FWM conversion efficiency for various values of nonlinear refractive index for (a) input pulses with low (weak) energies and (b) input pulses with high (strong) energies. The FWM conversion efficiency in the SOA is defined as the ratio of the generated FWM signal's power (energy) to the input power (energy) of the SOA in (dB) scale [19].

In the low power regime, the FWM conversion efficiency is varied from −54.9 dB to −53.2 dB when the value of nonlinear refractive index is varied from $-0.1\ cm^2/TW$ to $-1\ cm^2/TW$. But, in the high power regime, the FWM conversion efficiency is varied from −18.1 dB to −15.5 dB when the value of nonlinear refractive index is varied from $-0.1\ cm^2/TW$ to $-1\ cm^2/TW$.

In both conditions, the FWM conversion efficiency is increased when the absolute value of nonlinear refractive index is increased. The simulation results confirm that the FWM conversion efficiency has higher values in the high power regime. Moreover, the increasing rate of FWM conversion efficiency is faster in the high power regime. It has the same reason as explained in Fig. 6 and it is the nonlinear relationship between the intensity of the generated FWM signal and the intensity of input pump and probe pulses.

3.2. Refractive index

The variation of SOA's refractive index due to the propagation of ultra-short optical pulses through the SOA waveguide is also investigated. The relationship between the refractive index and the intensity of the propagated pulse is given by the following equation [6]:

$$n = n_0 + n_2 \times I \tag{14}$$

where n is the refractive index, n_0 is the linear refractive index, n_2 is the nonlinear refractive index and I is the optical intensity of the propagated pulse. Optical intensity is the optical power per unit area that is transmitted on the imagined plane perpendicular to the direction of propagation [6].

The intensity of the propagated pulse is spatially dependent on the refractive index. In other words, the refractive index of the waveguide is not constant and it changes during the propagation of optical pulse (wave).

To calculate the intensity of the propagated pulses, first we should calculate the power of the pulse in each section of the waveguide. Fig. 8 shows the power of propagated pulses at the beginning of the waveguide (L=0 μm), middle (L=250 μm) and end (L=500 μm) of the waveguide. It has been shown that propagated pulses reach their highest power at the end of the waveguide and the maximum power is 8.08 W, when the input pump and probe pulses energies are 5 pJ and 500 fJ, respectively. For low power regime, the peak output power of the propagated pulse is 68 mW.

Fig. 9 shows the value of refractive index in the SOA's waveguide for high power regime. To calculate the maximum intensity in each section of the waveguide, the highest power of the propagated pulse has been considered using the following

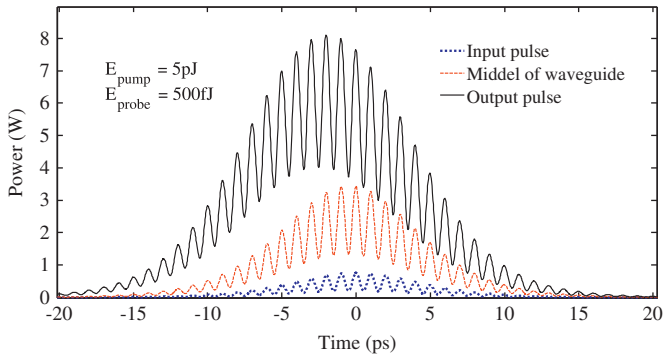

Fig. 8. Power of the propagated pulses at the beginning of the SOA waveguide (L=0 μm), middle of the SOA waveguide (L=250 μm) and at the end of the SOA waveguide (L=500 μm). Input pump and probe pulses energies are 5 pJ and 500 fJ, respectively.

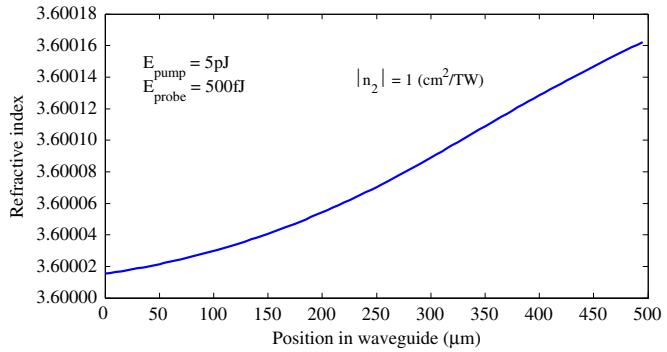

Fig. 9. Refractive index in each section of the waveguide during the propagation of optical pulses. The absolute value of nonlinear refractive index is 1 cm^2/TW and the modification of refractive index is not severe.

equation:

$$I_{max} = \frac{P_{max}}{A} \tag{15}$$

where P_{max} is the maximum propagated power in each section of the waveguide. The calculated intensity has been replaced in (14) and the obtained refractive index is shown in Fig. 9.

Fig. 9 indicates that the evolution of high power optical pulses with the FWHM of 10 ps and the nonlinear refractive index of $|n_2| = 1$ cm^2/TW has influenced the refractive index of the waveguide in the order of 10^{-4}.

For low power regime, the condition is the same as high power regime. However, the energy of the propagated pulse is weak and the variation of the nonlinear refractive index starts from the order of 10^{-7}.

4. Conclusions

In this work, we have analyzed the influences of nonlinear refractive index on the generated FWM signal characteristics in the SOA. We obtained that the generated FWM signal power is increased when the absolute value of the nonlinear refractive index is increased. In a high power (saturated gain) regime, when absolute value of the nonlinear refractive index is increased, the waveform (pulse shape) and the spectrum of the generated FWM signal experienced a peak shift to the trailing edge and leading edge, respectively. Moreover, the FWHM and the TBP of the generated FWM signals are decreased with the increase of the absolute value of nonlinear refractive index. Furthermore, the generated FWM signal energy (FWM conversion efficiency) is increased by increasing the absolute value of the nonlinear refractive indexes. So, increasing the FWM conversion efficiency is useful for the design of optimum wavelength converters. Besides, we have also studied the influence of propagation of optical pulses on the refractive index in the SOA. Based on our simulation results, we conclude that the small variation of the nonlinear refractive index can affect the FWM phenomena in the SOA and its effect is more tangible in the high power regime when the SOA is saturated.

References

[1] Geraghty DF, Lee RB, Verdiell M, Ziari M, Mathur A, Vahala KJ. Wavelength conversion for WDM communication systems using four-wave mixing in semiconductor optical amplifiers. IEEE Journal of Selected Topics in Quantum Electronics 2002;3:1146–55.
[2] Geraghty DF, Lee RB, Vahala KJ, Verdiell M, Ziari M, Mathur A. Wavelength conversion up to 18 nm at 10 Gb/s by four-wave mixing in a semiconductor optical amplifier. IEEE Photonics Technology Letters 1997;9(4).
[3] Connelly MJ. Semiconductor Optical Amplifiers. Boston, MA: Kluwer; 2002.
[4] Razaghi M, Ahmadi V, Connelly MJ. Femtosecond pulse shaping using counter-propagating pulses in a semiconductor optical amplifier. Optics Quantum Electronics, Springer 2009.
[5] Das NK, Yamayoshi Y, Kawazoe T, Kawaguchi H. Analysis of optical DEMUX characteristics based on four-wave mixing in semiconductor optical amplifiers. IEEE/OSA Journal of Lightwave Technology 2001;19(I2):237–46.
[6] R. Paschotta, Encyclopedia of Laser Physics and Technology, VILEY-VCH, vol. I, 2008.
[7] Hall KL, Thoen ER, Ippen EP. Semiconductors and Semimetals 1998;59: 83–160. Chapter II.
[8] Razaghi M, Ahmadi V, Connelly MJ. Comprehensive finite-difference time-dependent beam propagation model of counter-propagating picosecond pulses in a semiconductor optical amplifier. IEEE/OSA Journal of Lightwave Technology 2009;27(15):3162–74.
[9] Das NK, Yamayoshi Y, Kawaguchi H. Analysis of basic four-wave mixing characteristics in a semiconductor optical amplifier by the finite-difference beam propagation method. IEEE Journal of Quantum Electronics 2000;36(10): 1184–92.
[10] Hong MY, Chang YH, Dienes A, Heritage JP, Delfyett PJ, Dijaili S, Peterson FG. Femtosecond self- and cross-phase modulation in semiconductor laser amplifiers. IEEE Journal of Selected Topics on Quantum Electronics 1996;2: 523–39.
[11] Agrawal GP, Olsson NA. Self-phase modulation and spectral broadening of optical pulses in semiconductor laser amplifiers. IEEE Journal of Quantum Electronics 1989;25(11):435–42.
[12] Mecozzi A, Mork J. Saturation induced by picoseconds pulses in semiconductor optical amplifiers. Journal of the Optical Society of America B 1997;14(4):761–70.
[13] Tang JM, Shore KA. Active picoseconds optical pulse compression in semiconductor optical amplifiers. IEEE Journal of Quantum Electronics 1999;35(1): 93–100.
[14] Occhi L, Schares L, Guekos G. Phase modelling based on the α-factor in bulk semiconductor optical amplifiers. IEEE Journal of Selected Topics on Quantum Electronics 2003;9(3):788–97.
[15] Uskov A, Mork J, Mark J. Theory of short-pulse gain saturation in semiconductor laser amplifiers. IEEE Photonics Technology Letters 1992;4(5):443–6.
[16] Conte SD, de Boor C. Elementary Numerical Analysis: An Algorithmic Approach. 3rd ed. Singapore: McGraw-Hill Book Company Co.; 1981.
[17] Zhao G, Patent E, van der Tol JJGM. Modeling of optical nonlinearities based on engineering the semiconductor band. Materials Science in Semiconductor Processing 2003;6:153–8.
[18] Hurlbut WC, Lee Yun-Shik. Multiphoton absorption and nonlinear refraction of GaAs in the mid-infrared. Optics Letters 2007;32(6).
[19] Jianhui Z, Namkyoo P, Vahala KJ, Newkirk MA, Miller BI. Four-wave mixing wavelength conversion efficiency in semiconductor travelling-wave amplifiers measured to 65 nm of wavelength shift. IEEE Photonics Technology Letters 1994;6(8):984–7.
[20] Marple DTF. Refractive index of GaAs. Journal of Applied Physics 1964;35(4): 1241–2.